

Accepted manuscript

Attestog, S., Senanayaka, J. S. L., Huynh, V. K. & Robbersmyr, K. G. (2022). Robust Active Learning Multiple Fault Diagnosis of PMSM Drives with Sensorless Control under Dynamic Operations and Imbalanced Datasets. IEEE Transactions on Industrial Informatics, 1-11. <https://doi.org/10.1109/TII.2022.3227628>

Published in: IEEE Transactions on Industrial Informatics

DOI: <https://doi.org/10.1109/TII.2022.3227628>

AURA: <https://hdl.handle.net/11250/3053634>

Copyright: © 2022 IEEE

License:

© 2022 IEEE. Personal use of this material is permitted. Permission from IEEE must be obtained for all other uses, in any current or future media, including reprinting/republishing this material for advertising or promotional purposes, creating new collective works, for resale or redistribution to servers or lists, or reuse of any copyrighted component of this work in other works.

Robust Active Learning Multiple Fault Diagnosis of PMSM Drives with Sensorless Control under Dynamic Operations and Imbalanced Datasets

Sveinung Attestog, Jagath Sri Lal Senanayaka, *Member, IEEE*,
Huynh Van Khang, and Kjell G. Robbersmyr, *Senior Member, IEEE*

Abstract—This paper proposes an active learning scheme to detect multiple faults in permanent magnet synchronous motors in dynamic operations without using historical labelled faulty training data. The proposed method combines the self-supervised anomaly detector based on a local outlier factor (LOF) and a deep Q-network (DQN) supervised reinforcement learner to classify inter-turn short-circuit, local demagnetisation and mixed faults. The first fault, which is detected by LOF and verified by an expert during maintenance, is used as training data for the DQN classifier. From that point onward, the LOF anomaly detector and DQN fault classifiers are working in tandem in the identification of new faults, which require expert intervention when either of them identifies a fault. The robustness of the scheme against dynamic operations, mixed fault and imbalanced training datasets is validated via a comparative study using stray flux data from an in-house test setup.

Index Terms—Active learning, Demagnetisation, Imbalance classes, Inter-turn short-circuit, Permanent magnet synchronous motor, Mixed fault, Variable load and speed

I. INTRODUCTION

Permanent magnet synchronous motors (PMSM) in offshore wind turbines and electric vehicles are intensively exposed to mechanical and thermal stresses in dynamic operations with thermal cycling. These result in inter-turn short-circuit (ITSC), and local demagnetisation fault (DF) [1]. A local demagnetisation only affects a small region of rotor magnets in early states and induces a magnetic asymmetry in contrast to uniform DF, which downgrades all magnets equally. Detecting and identifying these faults in incipient stages allow for life-prolonging operation or planned maintenance, reducing costs and production down-times [2]–[4].

Fault detection and identification (FDI) methods for electrical machines have been extensively developed and categorised as: model-, signal- and machine learning (ML) based methods

This paragraph of the first footnote will contain the date on which you submitted your paper for review. It will also contain support information, including sponsor and financial support acknowledgment. For example, "This work was supported in part by the U.S. Department of Commerce under Grant BS123456."

The authors are with Department of Engineering Sciences, University of Agder, Jon Lilletuns vei 9, 4879 Grimstad, Norway (E-mail: sveinung.attedstog@uia.no, jagath.senanayaka@uia.no, huynh.khang@uia.no; kjell.g.robbersmyr@uia.no)

[5]. The model-based methods aim to identify fault signatures by estimating hard-to-measure parameters or computing a residual between a suggested model and measurements. This approach relies on the accurate information of physical parameters in the model or detailed dimensions of machines, which are difficult to acquire in reality [6]. Signal processing methods detect a fault based on fault-related characteristic frequencies. These methods are simple but are only applicable to single fault diagnosis. Further, missing a fault characteristic frequency does not guarantee that a machine is completely healthy. ML based methods have recently gained popularity since they are less demanding on prior knowledge of a machine and flexible in the implementation [7].

To address the lack of labelled faulty data issues, anomaly detection has been used in various studies [8]–[10]. These anomaly detectors and one-class classifiers (OCCs) train on the observation of healthy cases. A trained OCC can quantify the deviation of a new data sample from the healthy samples. A large deviation from a healthy sample is considered a faulty case. Krawczyk et. al. [11] separate the OCCs into four categories namely; (1) Density-based methods e.g. local outlier factor (LOF) [12], (2) Reconstruction-based methods e.g. auto-encoder [13] and contrastive learning [14], (3) Boundary-based methods e.g., one-class support vector machine (SVM) [15], (4) Ensemble-based methods which combine OCCs to form a more flexible data description model [11]. It is important to use a proper comparative study to find the best OCC type for a given anomaly detection application. However, to the authors' knowledge, finding the best OCC method for detecting an anomaly in PMSMs has not been studied in the literature.

Another method to tackle the lack of labelled faulty data is using active learning (AL). It is a set of semi-supervised learners [16], [17], which are used to accelerate the labelling process of a partially labelled dataset. They are trained on the labelled samples and tests on the unlabelled samples. The prediction with the lowest confidence is passed to an expert, who "actively" labels the dataset for the ML-based detection. An AL is often called a cooperative learner when it significantly alleviates the labelling task for the expert. Authors in [18] presented an ensemble-based fuzzy rough AL approach for detecting broken rotor bars in induction motors based on a data entropy criterion. It retrains a new classifier if the input samples have drifted. The proposed FDI scheme is robust

against non-stationary signals but requires the initial faulty samples for its implementation. The study in [8] proposed an FDI development scheme without using historical data from an operating electric powertrain with faults on gearbox, bearing and stator winding. Within the study, a self-supervised one-class SVM is first used to detect the anomaly. However, this OCC defines healthy domains based on its kernel function and may include regions of low competence. It will have a high rate of false negatives (FN) if the healthy and faulty classes overlap. The second part of the presented FDI scheme is a convolutional neural network (CNN) classifier, which is trained by samples identified by the one-class SVM and validated by an expert. Further development of such an FDI will create a more competent CNN with knowledge of faults, that have occurred. The authors in [8] trained and tested the FDI scheme on a balanced dataset alone. However, obtaining a balanced dataset for ML-based fault diagnosis methods is not feasible from PMSMs in offshore wind turbines. Developing a novel fault diagnosis must take the imbalance in datasets into consideration.

Imbalance in a dataset is often measured by the ratio (λ) between negative (healthy) and positive (faulty) samples. The problem of imbalanced dataset is amplified due to noise, overlap between classes, and if one class is represented by multiple clusters [19]. A common method for "rebalancing" the imbalanced dataset is to oversample the minority class and undersample the majority class with random sampling, generating new synthetic samples or extraction maximisation imputation-based class imbalanced learning [20]. The study in [21] presented a cost-sensitive AL using bidirectional gated recurrent neural network for fault diagnosis. The FDI scheme is designed for larger industrial plants and is verified with the Tennessee Eastman dataset. However, the proposed FDI scheme is not experimentally validated on imbalanced datasets. The suggested recurrent neural network needs samples in a sequence, where the fault occurred in the sequence. These samples will be hard to acquire in reality. A PMSM may operate with a fault in its incipient state, which can be used in the training process. The proposed FDI scheme addressed the imbalanced dataset problem by weighting the positive and negative samples. The weight function is time-dependent and requires instant information of the occurred fault, being difficult to determine. Authors in [13] proposed a self-supervised feature learning scheme for bearing fault in steady-state with less than 50 labelled training samples per class. A CNN is trained with augmented data to match the computed pseudo labels, which consist of statistical features and features extracted from an auto-encoder. This allows for rich feature mining from a small number of positive samples. The FDI can be effective against imbalanced datasets, but it is only verified for detecting single faults on PMSM operating in a steady-state.

This study aims to develop a novel scheme of mixed fault diagnosis of PMSM drives with sensorless control under dynamic operations while addressing the problems of imbalanced datasets using limited samples from faulty conditions. Within the framework, an anomaly detector is developed based on a LOF to define more complex domains in healthy cases to

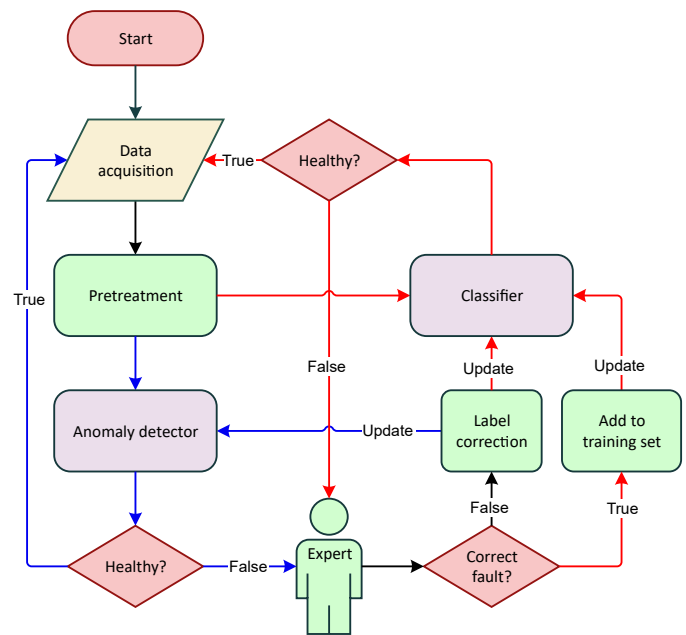


Fig. 1. Flowchart of the proposed FDI scheme. Note: Arrows coloured in red, blue and black represent information flow related to classifier, detector or both; Green objects represent processes/actions; purple boxes represent detector and classifier, and red diamonds represent decisions

tackle overlapping classes. The proposed scheme is proven to be robust against dynamic operations at different operation profiles. The OCC part of the proposed scheme is compared with the one-class SVM, while the DQN classifier is compared with the widely used ML classifiers, namely, two-class SVM, k-nearest neighbors (KNN) and CNN. This suggested scheme, using external flux sensors alone, allows for developing a plug-and-play automatic fault detection without modifying the existing drive systems in critical or offshore applications. The work flow of the research starts with collecting data from the in-house test setup. The PMSM is operating under three different operation profiles with the following fault cases: healthy, ITSC, DF and mixed fault (MF). Finally, the proposed scheme is trained and tested in anomaly detection, two- and four-class classifications.

II. PROPOSED FAULT DIAGNOSIS SCHEME

The proposed FDI scheme shown in Fig. 1 is developed based on an online fault diagnosis scheme in [8]. The pretreatment after data collection involves resampling of the original time-series data at a fixed angular increment. The resampled data are split into intervals of 30 revolutions, which are converted to the frequency domain by fast-Fourier transform (FFT). The spectrograms are normalised with respect to both the amplitude and frequency of the fundamental component. Then, the spectrograms are enveloped by splitting the spectrogram into intervals with a length of 0.5 order centred around the half harmonics (0.5, 1, 1.5, ...) to find the maximum in each interval. This saves storage space while maintaining the information on the half harmonics. The pretreatment makes the FDI scheme robust against dynamic operation conditions and can be implemented in drives with sensorless control.

Algorithm 1 Detailed description of FDI scheme

Require: Healthy case dataset, threshold, maintenance expert

while No discovered faulty cases **do**
 Compute Anomaly score with OCC
 if Anomaly criterion = TRUE **then:**
 Expert investigation
 if Fault = FALSE **then:**
 Update OCC
 else if Fault = TRUE **then**
 Perform maintenance
 Label discovered fault and train classifier
 end if
 end if
end while

while At least one discovered fault class **do**
 Compute Anomaly score with OCC
 Predict fault class with classifier
 if A fault is detected by classifier or OCC **then:**
 Expert investigation
 if Fault = TRUE **then:**
 Perform maintenance
 if Fault = New **then**
 Label dataset of new fault
 else if Fault = Old **then**
 Include new samples in fault dataset
 end if
 Update classifier
 else if Fault = FALSE **then**
 Update OCC
 end if
 end if
end while

The FDI scheme starts with detecting anomalies using a self-supervised anomaly detector since historical data at faulty conditions is not available. If the anomaly detector gives a false positive (FP), which is determined by an expert, it then needs to be updated with these FPs to learn the new region of the healthy case. True positive samples mark the end of the first stage of the FDI scheme since the samples of the faulty case are now available for training of the fault classifier. The second stage keeps the fault detector, but it works alongside the fault classifier. An investigation by an expert is required when either the detector or classifier identifies a fault. If a fault is detected and classified as a previously discovered fault, the fault search can be narrowed down during maintenance. Note that in the first iteration of stage 2, the classifier only knows of one fault. However, more data during operations will result in a more knowledgeable and confident FDI, which can speed up the maintenance process, and reducing unexpected downtime and cost. The detailed description of the FDI is given in Algorithm 1.

A. Estimation of rotor position

The input time-series samples $x(t)$ are resampled at a fixed angular increment based on the estimated value of rotor

position. It is estimated with an optimisation problem with the objective of minimising the square error between $x(t)$ and a sine function with respect to fundamental frequency f_1 and phase shift ϕ .

$$f_1, \phi = \min_{f_1, \phi} (x(t) - \sin(2\pi f_1 t + \phi))^2 \quad (1)$$

The input time-series data is split into samples of 0.1 s. The parameters f_1 are estimated for each sample. First, (1) is computed for $f_1 \in [0, 100]$ Hz with 5 Hz increments. The optimal ϕ is found for each f_1 with the golden section search. The combination of f_1 and ϕ yielding the smallest output of (1) is the initial guess in a simplex search method. The process is repeated to compute a function of f_1 over time, being integrated for acquiring the rotor position.

B. Anomaly detection

The existing anomaly detectors using self-supervised learners need samples from healthy cases to identify any anomalies, which later can be labelled by an expert for initiating the training of a fault classifier in a later stage. The suggested one-class SVM in [8] is replicated, and 10 % of the training data is assumed to be outliers. The drawback with this OCC is its assumption of defining the region of the healthy case with the kernel function. Regions of low competence may be included to increase the chance of FN. To address this demerit, a density-based method LOF in [12], [22] is used in this work to replace the one-class SVM. Like the k-nearest neighbours, the pair-wise distance between all the samples in the training dataset needs to be computed. This will make the LOF computationally heavy when the library of samples in the healthy case becomes too large. This problem can be solved by selective samplings [23].

The samples in the datasets are grouped into clusters. An outlier can be isolated by a threshold value of the average distance to its nearest neighbours. However, the samples of the healthy dataset do not necessarily have a uniform density in its cluster in feature space. Thus anomalies can be closer to a cluster, depending on the region in the feature space [12], [22]. LOF isolates outliers based on the sample density ρ_{samp} in feature space.

$$\rho_{\text{samp}}(P) = \left(\frac{1}{k} \sum_{n=1}^k d(P, o_n) \right)^{-1} \quad (2)$$

where k is an integer, $d(P, o_n)$ is the pair-wise Euclidean distance between point P and its nearest neighbours o_n . Then the sample density of each of the neighbour points o_n ($\rho_{\text{samp}}(o_n)$) needs to be computed. LOF is here defined as:

$$\text{LOF}(P) = \frac{1}{k} \sum_{n=1}^k \frac{\rho_{\text{samp}}(o_n)}{\rho_{\text{samp}}(P)} \quad (3)$$

Fig. 2 illustrates the principle of LOF. The sixth nearest neighbours for point P are coloured in orange, while the rest of the dataset is coloured in blue. Point o_1 is used as an example, where o_1 and its sixth nearest neighbours have grey connections. An anomaly is detected if LOF is greater

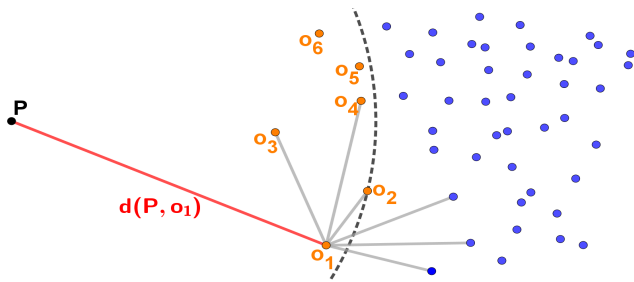


Fig. 2. Illustration of LOF in a 2D-feature space with P (black), o_n (orange), $d(P, o_1)$ (red), distance between o_1 to its nearest neighbours (grey), and rest of samples in the cluster (blue)

than a set threshold. This implies that the new observation P is located in a region, which is a too "sparsely" populated region in feature space.

C. Fault identification

After the anomaly detection, the multiple fault identifications are implemented by a reinforcement learning (RL) based classifier in this study. RL has already proven its effectiveness in information theory, simulation-based optimisation, control theory and statistics [24], [25] and developed for bearing fault diagnosis alone [26] while the imbalance issues were not addressed. The proposed RL scheme based on a double deep Q-network (DQN) in [27], [28] will be compared with the recently developed CNN architecture for fault identification in [8]. The problem with the existing CNN classifier is that it is not suited for imbalanced datasets. The proposed DQN fault classifier can compensate for the imbalanced datasets without any oversampling. RL usually uses the analogy of teaching the agent to play a game. In the fault classification, the RL agent plays a "quiz game". It is formulated in form of 1D arrays as features, where the agent needs to give a response on classification. The Q-learning aims to set up a Q-table that contains the policy to maximise a reward depending on the input. In DQN, the Q-table is replaced with a neural network. Fig. 3 illustrates the interaction between the DQN agent and its environment. The illustration inside the DQN shows the layers of the critic network with four layers: Input layer (243 nodes), fully connected layer (100 nodes), ReLU activation function layer and the second fully-connected layer. The number of nodes in the final layers is equal to the number of classes in the training data.

The action of the agent is associated with the label of the training dataset. If there are only two classes in the training set, it is sufficient to define the action space as $A = \{0, 1\}$. In this study, the action space is defined as $A = \{[0, 0], [0, 1], [1, 0], [1, 1]\}$. The entries in A represent healthy or no-fault (NF), DF, ITSC and MF, respectively. MF is the mix of DF and ITSC. The encoding of the labels is for the DQN only, which needs to be decoded after the prediction.

The reward function [27] is weighted based on the ratio between negative (healthy case) and positive (faulty case) samples.

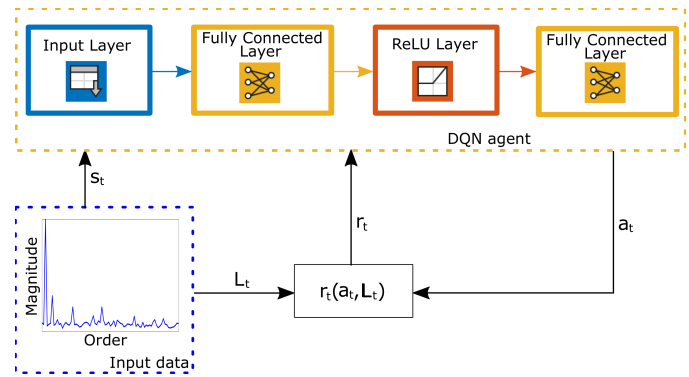


Fig. 3. Block diagram of DQN interacting with the environment

$$r_t = \begin{cases} 1, & a_t = L_t = \text{Negative} \\ -1, & a_t \neq L_t = \text{Negative} \\ \lambda, & a_t = L_t = \text{Positive} \\ -\lambda, & a_t \neq L_t = \text{Positive} \end{cases} \quad (4)$$

The performance of a classifier to identify positive samples will decline when the imbalance ratio λ is increased. Eventually, the network will classify every sample as negative regardless of input. This phenomenon is called a collapse and is caused by the fact that the negative samples receive a greater sway in the training of the network since they are in majority. The role of r_t is to tackle the trend towards a collapse by balancing the weights of the negative and positive samples in the training process. The training process of the DQN is described in Algorithm 2 [29], where Θ is the parameter critic and τ is the smoothing factor for updating the target critic, which has the parameter Θ_t . There is no terminal state for S_{t+1} .

III. EXPERIMENTAL SETUP AND DATA COLLECTION

A. In-house test bench

The studied four-pole, 2.2 kW PMSM is coupled to a generator with a torque transducer in between as shown in Fig. 4. The output of the generator is rectified by a three-phase full-bridge rectifier with a 500 μF capacitor bank connected across the output terminals, to remove the ripples of the DC output. The brake chopper is regulated by a PWM signal, which needs to be amplified by a factor of 4 due to the voltage amplitude insufficiency from the Microlabbox. The PWM signal is defined by the duty cycle, which in an ideal system would be proportional to the reciprocal of the motor speed. However, due to losses and imperfections, a look-up table is generated for the duty cycle. It dictates the required duty cycle for achieving a requested load in the speed range between 1000 rpm and 2000 rpm.

The solid state hall sensors, Type SS495A, measure the stray flux. The output of these sensors is linear and ratio-metric within the range $[-67, 67]$ mT and has a sensitivity of $31.25 \frac{\text{mV}}{\text{mT}}$. Two sensors were soldered to a Veroboard and wired to the Microlabbox, which delivers power to the sensors and records the measurement. The sensors could measure both tangential and radial components of the stray flux. Two sets

Algorithm 2 Training Algorithm for DQN**Require:** Positive and negative samples**for** N_{epi} episode **do** Pick a random sample s_1 from the training set**for** $N_{\text{step}-1}$ steps **do** **if** Exploration **then** Pick a random action a_t from A **else** $a_t = \arg \max_{a_t} Q(s_t, a_t | \Theta)$ **end if** Execute a_t and observe the reward r_t Randomly pick s_{t+1} from training set Store the experience (s_t, a_t, r_t, s_{t+1})

Compute and store the value function:

 $y_t = r_t + \gamma \max_{A_t} Q_t(s_{t+1}, a_{t+1} | \Theta_t)$. Compute the loss for a mini-batch with M samples

$$L = \frac{1}{M} \sum_{t=1}^M (y_t - Q(s_t, a_t | \Theta))^2$$

Update the critic by one-step minimisation

Update the target critic parameters with

$$\Theta_t = \tau \Theta + (1 - \tau) \Theta$$

Update the decaying probability for exploration

Repeat

end for**end for**

TABLE I

PARAMETERS OF THE MOTOR UNDER STUDY

| Parameter | Value |
|------------------|--------------|
| Output power | 2.2 kW |
| Nominal voltage | 280 V |
| Nominal current | 5 A |
| Nominal speed | 3000 rpm |
| Nominal torque | 7.0 Nm |
| Number of poles | 4 |
| Phase resistance | 0.8 Ω |
| Inductance | 6 mH |

of sensors were placed in proximity to the PMSM at the top and on the side.

B. Description of collected datasets

Stray fluxes are measured for three different non-stationary operating conditions with a sampling rate of 10 kHz. The time-series data is resampled with 400 samples per rotor revolution and split into samples with a length of 30 revolutions. Each sample is transformed into the frequency domain to produce the features for each observation used for the training and testing the proposed algorithm. The test setup is operated with the three operation profiles shown in Fig. 5. Profile 1 consists of a regular pattern, where the speed ramps up and down between 1000 rpm and 2000 rpm, and the load changes between 25 % and 75 % of the full load. Profile 2, which keeps the load constant at 60 % of the full load, while the speed changes with a randomly generated speed profile. Profile

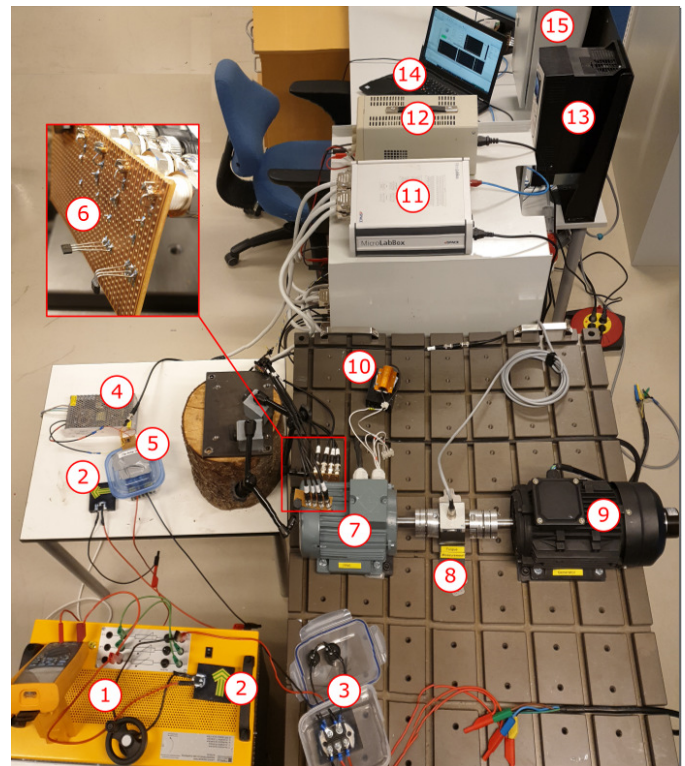


Fig. 4. Overview of the test bench with (1) resistor bank, (2) flyback diode, (3) three-phase rectifier with capacitor bank, (4) 12 V DC-supply, (5) IGBT brake chopper with OP-Amp, (6) hall sensors, (7) PMSM, (8) torque transducer, (9) generator, (10) short circuit resistor, (11) Microlabbox, (12) 24 V DC-supply, (13) ABB drive, (14) office laptop and (15) cabinet containing the current sensors

3 keeps the speed constant at 1200 rpm, and then the load is randomly generated, where it repeats itself every 30 s. Stray flux measurement was collected from the PMSM operating in all mentioned profiles in the following fault condition: NF, ITSC with 5 % severity, local partial DF, and an MF case with both ITSC and DF.

C. Implemented Faults

The local DFs in PMSM are usually implemented by removing parts of the magnets and replacing them with a non-magnetic material or installing weaker magnets in the rotor. These methods, however, do not mimic the local demagnetisation due to thermal cycling in dynamic operations of PMSM drives. In this study, one pole of the rotor is demagnetised by heating it on an electric hob for 10 minutes. Fig. 6 shows the heat-treatment of the rotor with a wet towel to prevent the other poles from demagnetisation. Fig. 7 shows the magnetic field strength of the demagnetised pole divided by the average field strength of the non-demagnetised poles after the heat treatment. The heat treatment caused two spots on one North pole to lose 30 % of their original strength. The heat treated rotor is installed in a PMSM stator during measurement of the PMSM with local DF, but it is replaced by an untreated rotor for measuring a non-demagnetised PMSM.

The studied PMSM has windings with three parallel wire strands per phase. This configuration reduces overall resistance, inductance, and back electromotive force. An analysis of

the equivalent resistance measured by a multi-meter is needed for estimating the number of shorted turns relative to the total number of turns per phase to define ITSC severity. Fig. 8 shows the PMSM with four short circuit taps implemented on separate wire strands in phase U. The ITSC is completed when it is connected to its input terminal in series with a short circuit resistor of 1Ω . The severity of the induced ITSC is estimated to short 5 % turns of a single wire strand. The remaining wire strands are not shorted.

IV. RESULTS AND DISCUSSIONS

A. Performance of anomaly detection

The one-class SVM and LOF need to define their respected criterion for anomaly identification. The sensitivity of the one-class SVM is defined by the outlier fraction, where the portion of outliers in the training dataset is set to 10 %. The output of the trained one-class SVM under testing is a numeric score, which is less than 0 in case of an anomaly as suggested in [8]. The LOF does require trial and error to determine a suitable threshold. A value close to 1 will make the detector more sensitive but has the risk of increasing the FP rate. The threshold for LOF was set to 1.1, which means that a new point is classified as an anomaly/fault if the regions of its k^{th} nearest neighbours are on average 10 % denser than the region of the new point. The parameter k is set to 5.

The one-class SVM and LOF classifiers are first trained on the healthy datasets from Profile 1 with the result shown in

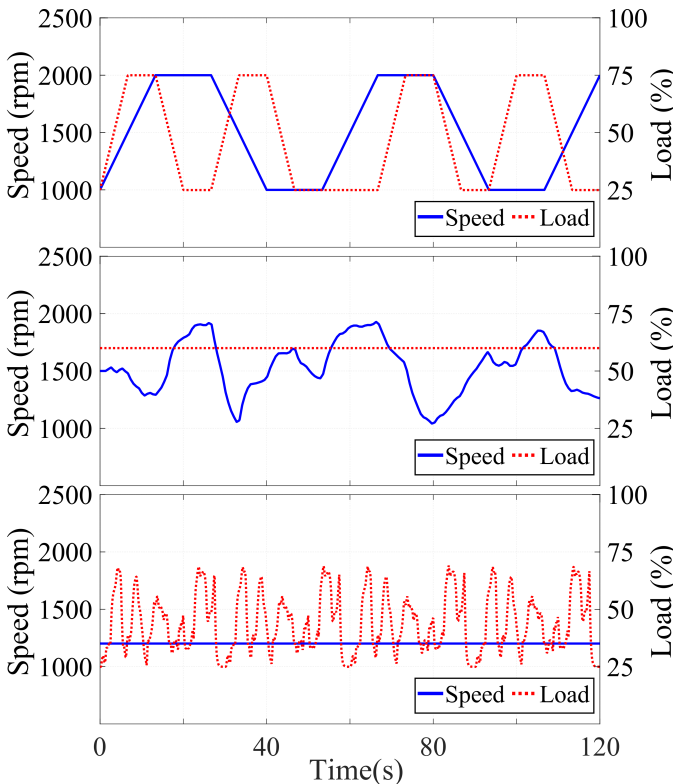


Fig. 5. The three studied operation profiles: (top) Profile 1 with variable load and variable speed, (middle) Profile 2 with constant load and variable speed, and (bottom) Profile 3 with variable load and constant speed



Fig. 6. Thermal treatment setup consisting of (1) cooking plate, (2) solid aluminium block, (3) wet towel and (4) the motor end shield

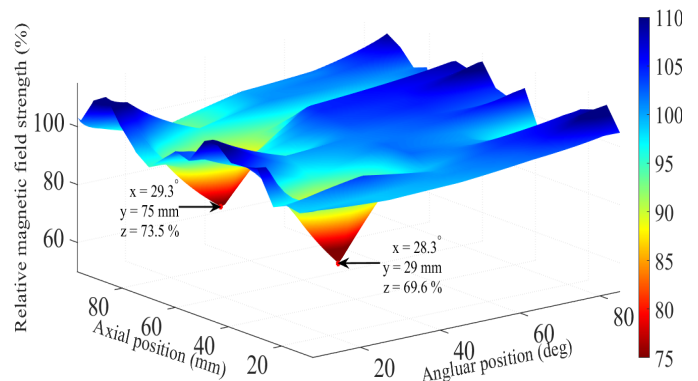


Fig. 7. Magnetic strength of faulty pole relative to healthy poles

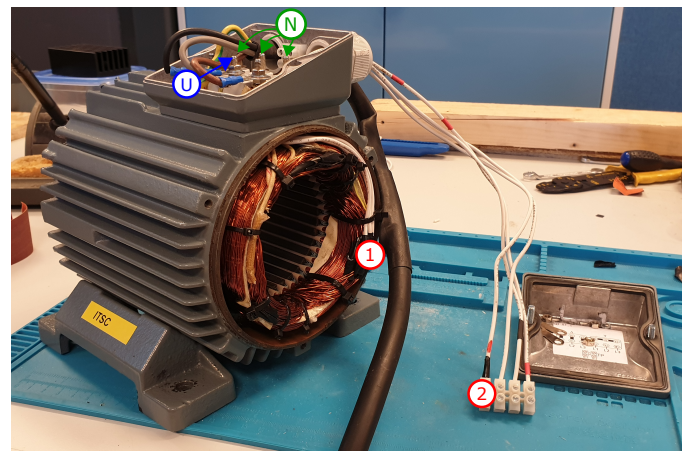


Fig. 8. The star connected PMSM with neutral point N is short-circuited with individual wire strands (1), which are accessed externally (2) and shorted with input terminate U

TABLE II
ACCURACY (%) OF ONE-CLASS SVM OUTLIER DETECTOR

| Fault test case (Criterion) | Test | Extra samples from Profile 2 and 3 | | | | | |
|--------------------------------|------|------------------------------------|------|------|------|------|------|
| | | Pro. | 0 | 50 | 100 | 150 | 200 |
| Healthy (Score ≥ 0) | 1 | 84.0 | 82.0 | 80.0 | 80.0 | 80.0 | 80.0 |
| | 2 | 80.0 | 98.0 | 98.0 | 98.0 | 98.0 | 98.0 |
| | 3 | 46.0 | 70.0 | 80.0 | 80.0 | 84.0 | 90.0 |
| DF (Score < 0) | 1 | 71.7 | 55.3 | 56.0 | 56.0 | 51.7 | 53.0 |
| | 2 | 57.0 | 46.0 | 45.7 | 44.3 | 41.0 | 41.0 |
| | 3 | 84.0 | 58.3 | 54.7 | 51.0 | 44.7 | 44.3 |
| ITSC (Score < 0) | 1 | 82.3 | 55.3 | 53.7 | 53.0 | 46.3 | 45.7 |
| | 2 | 90.7 | 54.3 | 48.0 | 39.7 | 22.7 | 21.7 |
| | 3 | 98.3 | 77.0 | 74.7 | 67.0 | 59.0 | 57.0 |
| MF (Score < 0) | 1 | 66.7 | 44.0 | 46.0 | 43.0 | 39.7 | 38.7 |
| | 2 | 73.3 | 32.0 | 30.3 | 23.7 | 16.3 | 15.0 |
| | 3 | 93.0 | 62.3 | 58.7 | 51.7 | 42.7 | 37.0 |

TABLE III
ACCURACY (%) OF LOF OUTLIER DETECTOR

| Fault test case (Criterion) | Test | Extra samples from Profile 2 and 3 | | | | | |
|--------------------------------|------|------------------------------------|------|------|------|------|------|
| | | Pro. | 0 | 50 | 100 | 150 | 200 |
| Healthy (LOF ≤ 1.1) | 1 | 86.0 | 86.0 | 88.0 | 88.0 | 80.0 | 98.0 |
| | 2 | 14.0 | 72.0 | 94.0 | 80.0 | 86.0 | 84.0 |
| | 3 | 8.0 | 52.0 | 88.0 | 80.0 | 82.0 | 90.0 |
| DF (LOF > 1.1) | 1 | 100 | 100 | 98.0 | 98.0 | 100 | 100 |
| | 2 | 100 | 98.0 | 100 | 100 | 100 | 100 |
| | 3 | 100 | 92.0 | 94.0 | 94.0 | 98.0 | 98.0 |
| ITSC (LOF > 1.1) | 1 | 100 | 100 | 100 | 100 | 100 | 100 |
| | 2 | 100 | 100 | 100 | 100 | 100 | 100 |
| | 3 | 100 | 100 | 100 | 94.0 | 100 | 100 |
| MF (LOF > 1.1) | 1 | 100 | 98.0 | 100 | 96.0 | 100 | 100 |
| | 2 | 100 | 94.0 | 96.0 | 100 | 100 | 98.0 |
| | 3 | 100 | 92.0 | 84.0 | 92.0 | 96.0 | 96.0 |

Table II and Table III. The healthy dataset was split by 83.3 % (250 samples) for training and 16.7 % (50 samples) for testing. All the samples from each of the faulty cases from any operation profile are used for testing (900 samples in total). Initially, the training set includes only samples from Profile 1. The performance of the one-class SVM has an accuracy of 84 % when tested on the same profile during training. The accuracy of the one-class SVM anomaly detector proposed in [8], when testing on each of the fault cases, varies between 57 % and 98.3 %. The proposed LOF algorithm, on the other hand, predicts all the fault cases as anomalies almost perfectly. However, the proposed LOF has a high FP rate. To address this issue, more samples in the healthy dataset from Profiles 2 (50 samples) and 3 (50 samples) are added to the training data to improve in the proposed FDI scheme with AL. As a result, the accuracy of the proposed LOF anomaly detector improves constantly when more samples are added. The compared one-class SVM detector suffers from the newly added data samples, where its accuracy in healthy cases improves, but the rate of FN increases. This proves that the proposed LOF anomaly detector could effectively identify anomalies better than the existing one when more knowledge of healthy cases is added during normal operations.

B. Training times of fault classifiers

To compare the computational effectiveness of the proposed DQN fault classifier, an existing one, the average training times

TABLE IV
RECORDED TRAINING TIME (S) OF DQN AND CNN

| Imb. | DQN | | CNN | |
|------|-----------|-----------|-----------|-----------|
| | 2 classes | 4 classes | 2 classes | 4 classes |
| 1 | 133.5 | 125.0 | 279.1 | 525.7 |
| 1.25 | 131.9 | 123.0 | 233.6 | 437.9 |
| 1.67 | 132.1 | 120.5 | 209.6 | 348.7 |
| 2.5 | 131.1 | 122.2 | 187.2 | 284.8 |
| 5 | 129.4 | 122.0 | 163.2 | 196.4 |
| 10 | 129.6 | 124.0 | 140.7 | 155.3 |
| 15 | 126.5 | 118.4 | 141.1 | 154.9 |
| 30 | 127.1 | 119.7 | 142.9 | 139.3 |

of DQN and the CNN benchmark are reported in Table IV while increasing the imbalance in the datasets. The classifiers were trained with two classes (healthy and faulty), and with all four classes of healthy, DF, ITSC and MF. The training time for the DQN stays close to constant around two minutes while the training time of the CNN declines when increasing the imbalance as reported in Table IV. The training times of the SVM and KNN classifiers are not included, because they are less than a few seconds. The imbalance ratio λ is increased by removing samples in the faulty case. The number of steps in each of the episodes in the DQN is set to 400, which would explain why the training time does not change. The CNN-based classifier on the other hand uses all available samples in each step in the training. It is noted that the imbalance of the training dataset in the case of four-class is computed by the imbalance of each respected fault class. The ratio between healthy and each faulty case is considered a more relevant metric in the compensation described in the reward function. In this study, equal imbalance (Imb.) ratios λ are applied for each fault case.

C. Performance of two-class classifiers

The proposed DQN and existing SVM, KNN and CNN fault classifiers use the half harmonics of the radial and tangential components of the stray flux as features. They all are trained to identify a specific single fault, namely DF or ITSC, which is indicated by the second line of Table V and Table VI. The number of nearest neighbours is set to 5 for the KNN. Results of true positive rate (TPR) and true negative rate (TNR) are listed in the tables. Values above 98 %, in green and red-coloured numbers indicate values below 50 %. This is to highlight the main trends of the results. The terms of positive and negative samples will hereafter be interchangeably used with faulty and healthy cases, respectively. The imbalance is increased by reducing the number of positive samples in the training dataset. All negative samples from the PMSM operating with Profile 1 are used for training. The test dataset from Profile 1 consists of 50 positive and 50 negative samples. The positive samples from each fault case are not sampled from the training dataset when $\lambda > 1$. All samples from Profile 2 and Profile 3 are used for testing (300 samples per health class per profile).

In the case of DF, only the samples of the motor with an induced local demagnetisation are used as the positive training samples. The proposed DQN and existing SVM, KNN and

TABLE V

TPR (%) AND TNR (%) OF SVM AND KNN CLASSIFIERS WHEN TRAINED FOR IDENTIFYING EITHER DF OR ITSC

| Test Pro. | Imb. ratio | SVM | | | | | | | | KNN | | | | | | | |
|-----------|------------|--------|--------|--------|----------|----------|--------|--------|--------|--------|--------|--------|----------|----------|--------|--------|--------|
| | | DF | | | | ITSC | | | | DF | | | | ITSC | | | |
| | | TPR DF | TNR NF | TPR MF | TNR ITSC | TPR ITSC | TNR NF | TPR MF | TNR DF | TPR DF | TNR NF | TPR MF | TNR ITSC | TPR ITSC | TNR NF | TPR MF | TNR DF |
| 1 | 1 | 98.4 | 99.1 | 93.7 | 28.7 | 100 | 100 | 71.3 | 89.3 | 98.6 | 100 | 82.3 | 44.7 | 100 | 100 | 70.0 | 89.3 |
| | 1.25 | 78.5 | 99.6 | 91.4 | 33.6 | 98.5 | 100 | 71.0 | 90.4 | 84.8 | 100 | 77.5 | 50.0 | 97.5 | 100 | 66.0 | 90.5 |
| | 1.67 | 73.9 | 99.8 | 89.1 | 34.8 | 97.6 | 100 | 69.5 | 91.0 | 71.0 | 100 | 69.4 | 57.8 | 93.1 | 100 | 60.9 | 92.9 |
| | 2.5 | 72.0 | 100 | 85.5 | 46.5 | 96.5 | 100 | 66.0 | 92.5 | 54.4 | 100 | 55.6 | 68.9 | 84.2 | 100 | 51.0 | 95.3 |
| | 5 | 60.9 | 100 | 74.3 | 57.0 | 91.9 | 100 | 56.5 | 94.8 | 22.7 | 100 | 28.5 | 85.5 | 68.2 | 100 | 32.1 | 98.0 |
| | 10 | 38.3 | 100 | 54.6 | 72.6 | 86.6 | 100 | 43.9 | 96.7 | 3.8 | 100 | 8.5 | 95.2 | 45.3 | 100 | 13.8 | 99.3 |
| | 15 | 32.3 | 100 | 45.9 | 78.6 | 78.9 | 100 | 33.6 | 97.1 | 2.2 | 100 | 3.5 | 97.7 | 29.3 | 100 | 8.0 | 99.6 |
| | 30 | 17.1 | 100 | 24.9 | 88.3 | 65.0 | 100 | 19.5 | 98.4 | 0.4 | 100 | 0.8 | 99.5 | 10.3 | 100 | 1.5 | 99.9 |
| 2 | 1 | 82.0 | 63.0 | 91.3 | 20.3 | 91.3 | 90.0 | 84.0 | 77.0 | 60.3 | 87.7 | 84.7 | 39.0 | 96.3 | 93.0 | 84.0 | 77.7 |
| | 1.25 | 80.6 | 64.5 | 89.1 | 28.3 | 91.1 | 91.1 | 82.7 | 78.3 | 48.9 | 91.4 | 74.4 | 48.7 | 94.3 | 95.5 | 81.0 | 81.4 |
| | 1.67 | 77.1 | 67.5 | 86.3 | 33.1 | 90.0 | 92.2 | 82.8 | 78.5 | 39.1 | 94.7 | 62.7 | 59.7 | 92.1 | 96.9 | 76.9 | 84.9 |
| | 2.5 | 71.1 | 72.7 | 81.8 | 39.2 | 88.4 | 92.8 | 78.7 | 82.4 | 23.7 | 96.7 | 46.3 | 71.7 | 85.7 | 98.5 | 68.9 | 90.2 |
| | 5 | 58.7 | 80.4 | 68.8 | 56.2 | 82.4 | 96.0 | 73.1 | 86.3 | 7.1 | 99.1 | 14.6 | 89.9 | 61.4 | 99.8 | 45.2 | 97.7 |
| | 10 | 43.9 | 87.0 | 52.3 | 68.2 | 73.6 | 98.1 | 61.2 | 91.9 | 2.2 | 99.9 | 6.0 | 95.7 | 30.0 | 100 | 19.5 | 99.7 |
| | 15 | 36.9 | 90.3 | 46.9 | 73.9 | 63.6 | 98.6 | 49.8 | 93.4 | 0.4 | 99.9 | 1.3 | 98.6 | 17.2 | 100 | 9.0 | 99.9 |
| | 30 | 19.2 | 95.4 | 29.0 | 83.0 | 43.6 | 99.5 | 33.0 | 97.0 | 0.1 | 100 | 0.3 | 99.6 | 3.0 | 100 | 0.9 | 100 |
| 3 | 1 | 74.0 | 75.0 | 87.7 | 48.0 | 96.0 | 95.3 | 80.1 | 83.0 | 38.7 | 86.0 | 52.7 | 23.7 | 93.0 | 98.0 | 30.3 | 95.7 |
| | 1.25 | 72.5 | 76.4 | 84.3 | 55.3 | 94.9 | 95.5 | 77.5 | 84.8 | 32.3 | 88.3 | 43.9 | 28.2 | 90.8 | 98.3 | 25.6 | 97.0 |
| | 1.67 | 68.9 | 78.6 | 80.5 | 58.5 | 93.4 | 96.6 | 74.6 | 86.9 | 21.1 | 92.8 | 31.0 | 35.4 | 87.2 | 99.0 | 19.1 | 98.0 |
| | 2.5 | 68.4 | 80.5 | 79.5 | 59.0 | 92.4 | 97.3 | 68.7 | 89.6 | 10.5 | 96.9 | 13.5 | 42.8 | 81.6 | 99.7 | 14.2 | 99.3 |
| | 5 | 55.2 | 89.1 | 65.0 | 65.2 | 88.0 | 98.6 | 57.3 | 94.0 | 2.7 | 99.5 | 4.2 | 65.4 | 65.0 | 99.9 | 7.3 | 99.8 |
| | 10 | 31.5 | 95.4 | 40.7 | 73.8 | 71.9 | 99.5 | 36.2 | 96.9 | 0.7 | 99.8 | 0.5 | 85.2 | 34.8 | 100 | 1.9 | 100 |
| | 15 | 27.2 | 96.0 | 36.4 | 76.0 | 72.7 | 99.8 | 28.3 | 97.9 | 0.2 | 99.9 | 0.2 | 93.8 | 24.5 | 100 | 1.0 | 100 |
| | 30 | 10.6 | 98.5 | 15.5 | 86.4 | 49.6 | 100 | 11.5 | 99.8 | 0.1 | 100 | 0.1 | 97.0 | 6.7 | 100 | 0.2 | 100 |

TABLE VI

TPR (%) AND TNR (%) OF DQN AND CNN CLASSIFIERS WHEN TRAINED FOR IDENTIFYING EITHER DF OR ITSC

| Test Pro. | Imb. ratio | DQN | | | | | | | | CNN | | | | | | | |
|-----------|------------|--------|--------|--------|----------|----------|--------|--------|--------|--------|--------|--------|----------|----------|--------|--------|--------|
| | | DF | | | | ITSC | | | | DF | | | | ITSC | | | |
| | | TPR DF | TNR NF | TPR MF | TNR ITSC | TPR ITSC | TNR NF | TPR MF | TNR DF | TPR DF | TNR NF | TPR MF | TNR ITSC | TPR ITSC | TNR NF | TPR MF | TNR DF |
| 1 | 1 | 100 | 99.9 | 95.8 | 100 | 98.5 | 97.9 | 12.8 | 99.4 | 97.2 | 98.4 | 73.7 | 99.9 | 95.4 | 96.6 | 2.9 | 99.8 |
| | 1.25 | 100 | 99.9 | 97.6 | 99.8 | 95.7 | 97.2 | 9.4 | 99.6 | 96.3 | 98.1 | 71.2 | 99.9 | 93.2 | 93.6 | 6.7 | 98.6 |
| | 1.67 | 100 | 99.7 | 99.6 | 100 | 97.1 | 98.1 | 11.5 | 98.8 | 95.8 | 98.9 | 71.0 | 100 | 89.1 | 97.9 | 5.8 | 98.8 |
| | 2.5 | 100 | 99.9 | 99.5 | 98.8 | 98.2 | 96.5 | 14.9 | 98.4 | 95.5 | 99.3 | 69.8 | 99.9 | 81.6 | 97.9 | 1.6 | 99.9 |
| | 5 | 100 | 98.7 | 99.6 | 99.1 | 96.4 | 95.6 | 14.7 | 98.9 | 92.9 | 98.6 | 64.3 | 99.9 | 67.6 | 96.9 | 2.1 | 99.8 |
| | 10 | 100 | 96.1 | 99.9 | 97.9 | 96.2 | 92.8 | 19.0 | 97.7 | 82.1 | 99.8 | 49.8 | 100 | 55.4 | 96.7 | 3.0 | 99.7 |
| | 15 | 99.9 | 93.4 | 99.6 | 95.8 | 93.4 | 90.3 | 15.7 | 98.5 | 69.4 | 97.5 | 35.8 | 99.7 | 43.5 | 99.7 | 2.0 | 99.5 |
| | 30 | 100 | 88.6 | 100 | 93.1 | 90.1 | 84.7 | 27.2 | 95.5 | 46.9 | 99.8 | 23.9 | 99.9 | 23.6 | 99.7 | 0.2 | 100 |
| 2 | 1 | 99.4 | 100 | 95.8 | 99.9 | 91.4 | 85.1 | 28.9 | 95.4 | 92.3 | 93.4 | 74.3 | 99.4 | 80.0 | 94.0 | 3.0 | 99.9 |
| | 1.25 | 99.6 | 99.9 | 97.9 | 100 | 92.7 | 85.1 | 24.6 | 96.6 | 94.8 | 93.7 | 77.1 | 99.5 | 77.8 | 91.0 | 4.8 | 99.7 |
| | 1.67 | 99.9 | 99.6 | 98.8 | 100 | 90.0 | 85.7 | 24.9 | 96.2 | 95.3 | 93.2 | 75.8 | 99.4 | 72.8 | 95.1 | 4.4 | 99.6 |
| | 2.5 | 99.8 | 99.1 | 99.5 | 99.7 | 94.6 | 77.9 | 35.1 | 92.3 | 95.2 | 94.8 | 75.9 | 99.4 | 65.0 | 95.9 | 2.0 | 100 |
| | 5 | 99.9 | 97.9 | 99.6 | 99.3 | 94.4 | 72.5 | 35.7 | 91.2 | 91.3 | 95.0 | 65.8 | 99.5 | 47.4 | 96.4 | 1.7 | 99.9 |
| | 10 | 99.9 | 91.6 | 99.8 | 96.4 | 88.0 | 69.9 | 35.1 | 91.7 | 75.4 | 97.5 | 47.3 | 99.9 | 37.6 | 96.3 | 1.4 | 99.8 |
| | 15 | 100 | 85.0 | 99.9 | 93.8 | 84.6 | 68.8 | 30.7 | 91.2 | 66.7 | 93.2 | 37.6 | 98.6 | 23.4 | 99.4 | 0.6 | 99.8 |
| | 30 | 100 | 72.8 | 100 | 89.8 | 79.6 | 72.3 | 33.2 | 88.0 | 49.1 | 97.6 | 32.2 | 99.3 | 13.2 | 99.5 | 0.3 | 100 |
| 3 | 1 | 97.9 | 99.9 | 89.0 | 100 | 82.0 | 91.6 | 12.4 | 99.3 | 99.0 | 97.1 | 91.6 | 100 | 76.1 | 94.6 | 5.4 | 99.1 |
| | 1.25 | 97.8 | 99.9 | 90.9 | 100 | 83.2 | 90.2 | 10.1 | 99.3 | 98.5 | 95.4 | 90.8 | 99.7 | 81.0 | 87.9 | 11.8 | 96.9 |
| | 1.67 | 98.9 | 99.8 | 94.0 | 99.9 | 83.8 | 90.1 | 10.9 | 99.3 | 99.1 | 96.4 | 93.7 | 100 | 76.9 | 94.6 | 9.4 | 96.6 |
| | 2.5 | 99.5 | 98.2 | 96.5 | 99.5 | 85.9 | 87.7 | 11.4 | 99.0 | 98.3 | 98.0 | 88.1 | 99.8 | 64.4 | 97.1 | 2.0 | 99.9 |
| | 5 | 99.6 | 97.0 | 97.5 | 98.9 | 86.6 | 84.8 | 11.4 | 98.8 | 97.5 | 97.6 | 85.9 | 99.8 | 53.9 | 95.3 | 2.0 | 99.8 |
| | 10 | 99.8 | 93.1 | 98.4 | 97.8 | 86.9 | 80.2 | 14.1 | 98.8 | 88.4 | 99.6 | 71.0 | 100 | 39.1 | 95.9 | 1.9 | 99.1 |
| | 15 | 99.7 | 88.4 | 98.4 | 96.3 | 85.2 | 79.0 | 13.3 | 98.2 | 78.0 | 96.3 | 57.2 | 98.6 | 22.5 | 98.4 | 2.6 | 99.0 |
| | 30 | 99.8 | 82.2 | 99.1 | 95.1 | 83.9 | 73.2 | 20.5 | 95.0 | 46.8 | 99.6 | 30.8 | 100 | 18.2 | 99.3 | 0.4 | 100 |

CNN classifiers are tested on all four-fault cases, namely DF, ITSC, MF and NF or healthy, to investigate whether the two other faulty datasets (ITSC and MF) can be classified. The fault signatures of MF may share common characteristics with both DF and ITSC. Therefore, it is possible for the MF samples to be classified as a fault by the classifier trained for detecting DF or ITSC, which is why Table VI reports TPR for MF. Ideally, ITSC fault will not be classified as a fault by the classifiers trained for DF and vice versa. This is why Table VI reports TNR for the fault classifiers, which are not trained before being used in testing. Table V shows that both SVM and KNN classifiers have a high TPR for detecting DF when they are trained with the DF dataset, but the TPR drops when λ increases. In the case of balanced datasets, the TNR of classifiers for ITSC is below 30%. This rate increases with a greater λ , since the classifiers collapse and could not improve overall accuracy. The SVM and KNN classifiers are also less robust against the operation profiles, which were not included in the training dataset. Their accuracy drops significantly when being tested on Profile 2 and Profile 3.

The proposed DQN classifier and CNN achieve a TPR higher than 90% for the fault cases they are trained before testing when $\lambda = 1$. The lowest TPRs for the proposed DQN and compared CNN classifier are 82.0% and 76.1%, respectively when they were trained for the ITSC dataset and tested on profile 3 with a constant speed and variable load. The DQN classifier maintains a TPR of above 97.8% when trained and tested for DF. However, the TNR for the healthy case is dropping to 72.8%. The CNN classifier improves its TNR for the healthy case when increasing the imbalance of the datasets. Fewer FPs is normally a positive quality in a classifier, but TPR for the CNN drops to below 50% when increasing the imbalance in the dataset. The accuracy trend for the CNN classifier is reduced significantly when all samples are classified as healthy cases. The proposed DQN classifier, on the other hand, reduces the possibility of FN but has overcompensated slightly and increased FPs. Neither FP nor FN is desirable in FDI. However, both FN and FP rates can be compensated in the proposed AL scheme by correcting relabel by an expert, and the proposed DQN fault classifier has a second option with the weighted reward function.

The MF case includes both DF and ITSC. Therefore, there is a possibility that this fault case can be classified as one of those faults. This is in the context of fault classifiers, that are trained for identifying the presence of a specific fault. The test result reveals that both DQN and CNN classifiers, which are trained for DF, identify MF as a fault. The TPR reported under MF is lower as compared to the case, where the classifiers are trained and tested on the same fault case. The TPR for the CNN classifier is also reduced when increasing the imbalance in the datasets. Neither DQN nor CNN classifier identifies MF as a fault when they are trained to identify ITSC fault. This result indicates that there is a high possibility that DF and MF may share the same fault signatures. The fault classifier, being trained on all four fault cases included in this study, may find it difficult to distinguish between DF and MF. In the case of MF, SVM and KNN classifiers have a larger TPR than DQN and SVM classifiers, but their TPR drops with a greater imbalance

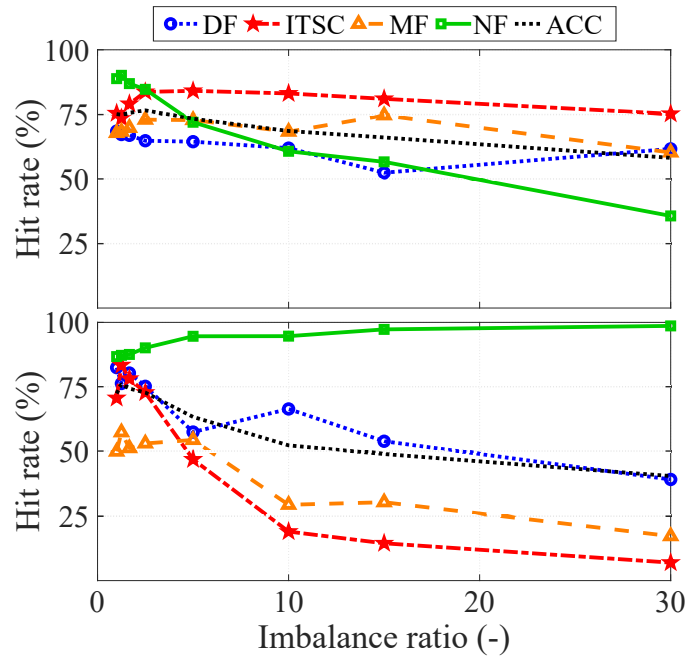


Fig. 9. Hit rates of DQN (top) and CNN (bottom) fault classifiers

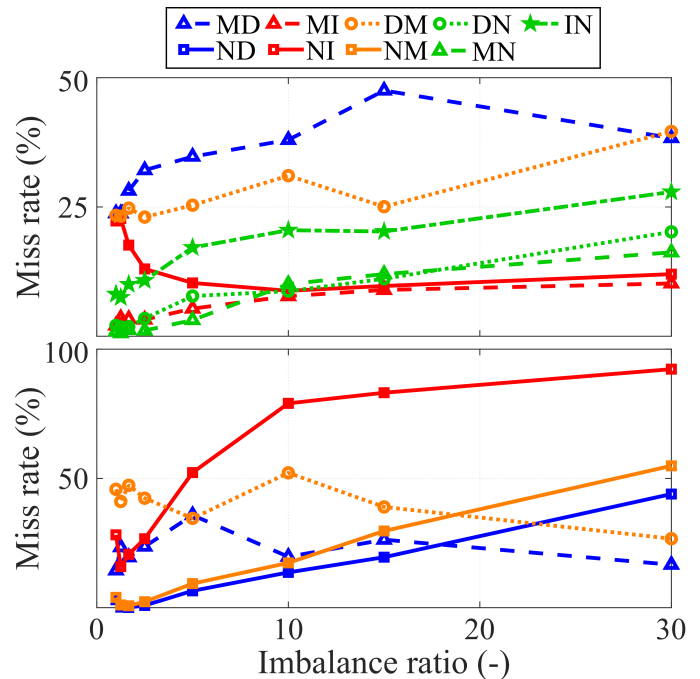


Fig. 10. Miss rates of DQN (top) and CNN (bottom) fault classifiers

in the dataset. This is the case when the classifiers are trained for classifying ITSC. The SVM and KNN classifiers are able to identify common signatures between ITSC and the MF, which are not present in DF.

D. Performance of four-class classifier

The proposed DQN and CNN fault classifiers are further trained with all four fault classes: DF, ITSC, MF and NF. KNN and SVM algorithms are not effective in classification of imbalanced datasets, and are not included in the four-class

classifier case study. Fig. 9 shows the hit rates (TPR and TNR) of the DQN and CNN fault classifiers using test dataset in Profile 3. This includes the TNR and TPR, which were discussed in Section IV.C. The overall accuracy is also added in Fig. 9, which is the average of the four hit rates, since the test dataset is balanced between the four classes. The proposed DQN and CNN fault classifiers suffer from being trained for all four faults. They start with an overall accuracy of 75 %, then decrease with respect to the imbalance of the dataset. Note each fault class has equal λ , which is the imbalance ratio given on the horizontal axis. The performance of the CNN is worse than the DQN, since its accuracy declines at a larger rate with a trend towards a collapse. Its hit rate for healthy case, i.e. NF, is increased towards 100 % due to this trend.

Each fault class can be incorrectly classified into three classes. This in total gives 12 miss rates (false positive rates and false negative rates) for a four-class classifier. Fig. 10 plots the miss rates for both DQN and CNN fault classifiers, which were not close to 0. The comparison still uses the test dataset from Profile 3. The first and last letters in the labels denote the predicted and true classes, respectively. Fig. 10 (top) reveals that the proposed DQN fault classifier is confused between DF and MF, which were predicted in the analysis of the two-class classifiers. The DQN classifier confuses ITSC with NF and MF, while NF is generally confused with all of the other health classes. This demonstrates that the reward function may have overcompensated and needs to be adjusted. A combined decision between fault classifier and anomaly detector may also reduce the rate of FPs since Table III reports a high accuracy for LOF. The CNN fault classifier does not misclassify NF with any of the fault classes. The confusion between DF and MF does decrease when increasing the imbalance, but these fault classes start to be predicted as NF instead. Almost all samples from fault case ITSC are misclassified as NF.

V. CONCLUSION

This study proposed a fault diagnosis scheme trained and tested with both dynamic operating conditions and mixed faults, where labelled training samples from the faulty conditions were initially unavailable. The training and testing datasets are collected from the in-house test setup with externally installed hall sensors. The proposed method order-normalises the spectrogram by resampling the time-series data at a fixed angular increment to make it more robust against dynamic operations. The rotor position is estimated with a single external stray flux sensor, which allows for an automatic fault diagnosis without modifying the existing PMSM drives with sensorless control. The LOF anomaly detector was trained on samples from Profile 1 with various operating conditions, which gave a high false positive rate. Nevertheless, the proposed active learning framework allows for improving prediction accuracy when adding new healthy case samples. Newly discovered health classes are used to train the proposed DQN classifiers at different imbalance ratios. The comparative study shows that the DQN fault classifier is more robust than the existing SVM, KNN and CNN fault classifier,

which were tested against the dynamic operations in Profile 2 and Profile 3. The DQN did overcompensate the weight of the minority class, being a new problem to be solved in future work. A reward function with a different ratio might yield higher accuracy. One possible solution is to integrate this parameter as an adjustable state variable in the training process of an agent. Furthermore, testing the performance of the proposed fault diagnosis scheme on other common faults, such as bearing or semiconductor switch faults, would be an interesting topic in the future studies.

REFERENCES

- [1] Y. Qi, E. Bostanci, V. Gurusamy, and B. Akin, "A Comprehensive Analysis of Short-Circuit Current Behavior in PMSM Interturn Short-Circuit Faults," *IEEE Transactions on Power Electronics*, vol. 33, no. 12, pp. 10 784–10 793, Dec. 2018, doi: 10.1109/TPEL.2018.2809668.
- [2] L. Wu, Y. Du, Z. Chen, Y. Guo, H. Wen, and Y. Fang, "Influence of Load Characteristics on Three-Phase Short Circuit and Demagnetization of Surface-Mounted PM Synchronous Motor," *IEEE Transactions on Industry Applications*, vol. 56, no. 3, pp. 2427–2440, Jan. 2020, doi: 10.1109/TIA.2020.2968036.
- [3] M. E. Iglesias Martínez, J. A. Antonino-Daviu, P. F. de Córdoba, J. A. Conejero, and L. Dunai, "Automatic Classification of Winding Asymmetries in Wound Rotor Induction Motors Based on Bicoherence and Fuzzy C-Means Algorithms of Stray Flux Signals," *IEEE Transactions on Industry Applications*, vol. 57, no. 6, pp. 5876–5886, Nov.-Dec. 2021, doi: 10.1109/TIA.2021.3108413.
- [4] I. Zamudio-Ramirez, R. A. Osornio-Rios, J. A. Antonino-Daviu, H. Razik, and R. d. J. Romero-Troncoso, "Magnetic Flux Analysis for the Condition Monitoring of Electric Machines: A Review," *IEEE Transactions on Industrial Informatics*, vol. 18, no. 5, pp. 2895–2908, Apr. 2021, doi: 10.1109/TII.2021.3070581.
- [5] E. A. Bhuiyan, M. M. A. Akhand, S. K. Das, and et. al., "A Survey on Fault Diagnosis and Fault Tolerant Methodologies for Permanent Magnet Synchronous Machines," *Int. J. Autom. Comput.*, vol. 17, no. 6, pp. 763–787, Dec. 2020, doi: 10.1007/s11633-020-1250-3.
- [6] Y. Qi, E. Bostanci, M. Zafarani, and B. Akin, "Severity Estimation of Interturn Short Circuit Fault for PMSM," *IEEE Transactions on Industrial Electronics*, vol. 66, no. 9, pp. 7260–7269, Sept. 2019, doi: 10.1109/tie.2018.2879281.
- [7] D. Neupane and J. Seok, "Bearing Fault Detection and Diagnosis Using Case Western Reserve University Dataset With Deep Learning Approaches: A Review," *IEEE Access*, vol. 8, pp. 93 155–93 178, Apr. 2020, doi: 10.1109/ACCESS.2020.2990528.
- [8] J. S. L. Senanayaka, H. V. Khang, and K. G. Robbersmyr, "Toward Self-Supervised Feature Learning for Online Diagnosis of Multiple Faults in Electric Powertrains," *IEEE Transactions on Industrial Informatics*, vol. 17, no. 6, pp. 3772–3781, Aug. 2021, doi: 10.1109/TII.2020.3014422.
- [9] C.-F. Tsai and W.-C. Lin, "Feature Selection and Ensemble Learning Techniques in One-Class Classifiers: An Empirical Study of Two-Class Imbalanced Datasets," *IEEE Access*, vol. 9, pp. 13 717–13 726, Jan. 2021, doi: 10.1109/ACCESS.2021.3051969.
- [10] K. Choi, J. Yi, C. Park, and S. Yoon, "Deep learning for anomaly detection in time-series data: Review, analysis, and guidelines," *IEEE Access*, vol. 9, pp. 120 043–120 065, 8 2021.
- [11] B. Krawczyk, M. Galar, M. Woźniak, H. Bustince, and F. Herrera, "Dynamic ensemble selection for multi-class classification with one-class classifiers," *Pattern Recognition*, vol. 83, pp. 34–51, Nov. 2018, doi = 10.1016/j.patcog.2018.05.015.
- [12] S. Liu, Y. Zhao, Z. Lin, Y. Liu, Y. Ding, L. Yang, and S. Yi, "Data-Driven Event Detection of Power Systems Based on Unequal-Interval Reduction of PMU Data and Local Outlier Factor," *IEEE Transactions on Smart Grid*, vol. 11, no. 2, pp. 1630–1643, Mar. 2020, doi: 10.1109/TSG.2019.2941565.
- [13] T. Zhang, J. Chen, S. He, and Z. Zhou, "Prior Knowledge-Augmented Self-Supervised Feature Learning for Few-shot Intelligent Fault Diagnosis of Machines," *IEEE Transactions on Industrial Electronics*, Jan. 2022, doi: 10.1109/TIE.2022.3140403.
- [14] Y. Ding, J. Zhuang, P. Ding, and M. Jia, "Self-supervised pretraining via contrast learning for intelligent incipient fault detection of bearings," *Reliability Engineering and System Safety*, vol. 218, p. 108126, Feb. 2022, doi: 10.1016/j.ress.2021.108126.

- [15] Y. Ji and H. Lee, "Event-based anomaly detection using a one-class svm for a hybrid electric vehicle," *IEEE Transactions on Vehicular Technology*, vol. 71, no. 6, pp. 6032–6043, May 2022.
- [16] C. Huang, "Featured Anomaly Detection Methods and Applications," Doctor of Philosophy in Computer Science, University of Exeter, Jun. 2018. [Online]. Available: <http://hdl.handle.net/10871/34351>
- [17] M. Chen, K. Zhu, R. Wang, and D. Niyato, "Active Learning-Based Fault Diagnosis in Self-Organizing Cellular Networks," *IEEE Communications Letters*, vol. 24, no. 8, pp. 1734–1737, Aug. 2020, doi: 10.1109/LCOMM.2020.2991449.
- [18] Z. Hosseinpour, M. M. Arefi, N. Mozafari, H. Luo, and S. Yin, "An ensemble-based fuzzy rough active learning approach for broken rotor bar detection in nonstationary environment," *IEEE Transactions on Instrumentation and Measurement*, vol. 71, pp. 1–8, May 2022.
- [19] Y. Lu, Y.-M. Cheung, and Y. Y. Tang, "Bayes Imbalance Impact Index: A Measure of Class Imbalanced Data Set for Classification Problem," *IEEE Transactions on Neural Networks and Learning Systems*, vol. 31, no. 9, pp. 3525–3539, Sept. 2020, doi: 10.1109/TNNLS.2019.2944962.
- [20] R. Razavi-Far, M. Farajzadeh-Zanjani, and M. Saif, "An Integrated Class-Imbalanced Learning Scheme for Diagnosing Bearing Defects in Induction Motors," *IEEE Transactions on Industrial Informatics*, vol. 13, no. 6, pp. 2758–2769, Dec. 2017, doi: 10.1109/TII.2017.2755064.
- [21] P. Peng, W. Zhang, Y. Zhang, Y. Xu, H. Wang, and H. Zhang, "Cost sensitive active learning using bidirectional gated recurrent neural networks for imbalanced fault diagnosis," *Neurocomputing*, vol. 407, pp. 232–245, Sept. 2020.
- [22] S. Luan, Z. Gu, L. B. Freidovich, L. Jiang, and Q. Zhao, "Out-of-distribution detection for deep neural networks with isolation forest and local outlier factor," *IEEE Access*, vol. 9, pp. 132 980–132 989, Aug. 2021.
- [23] M. E. Khoda, T. Imam, J. Kamruzzaman, I. Gondal, and A. Rahman, "Robust Malware Defense in Industrial IoT Applications Using Machine Learning With Selective Adversarial Samples," *IEEE Transactions on Industry Applications*, vol. 56, no. 4, pp. 4415–4424, July-Aug. 2020, doi: 10.1109/TIA.2019.2958530.
- [24] B. Jang, M. Kim, G. Harerimana, and J. W. Kim, "Q-Learning Algorithms: A Comprehensive Classification and Applications," *IEEE Access*, vol. 7, pp. 133 653–133 667, Sept. 2019, doi: 10.1109/access.2019.2941229.
- [25] Z. Song, J. Yang, X. Mei, T. Tao, and M. Xu, "Deep reinforcement learning for permanent magnet synchronous motor speed control systems," *Neural Computing and Applications*, vol. 33, no. 10, pp. 5409–5418, May 2021, doi: 10.1007/s00521-020-05352-1.
- [26] L. Wen, X. Li, and L. Gao, "A New Reinforcement Learning Based Learning Rate Scheduler for Convolutional Neural Network in Fault Classification," *IEEE Transactions on Industrial Electronics*, vol. 68, no. 12, pp. 12 890–12 900, Dec. 2021, doi: 10.1109/tie.2020.3044808.
- [27] E. Lin, Q. Chen, and X. Qi, "Deep reinforcement learning for imbalanced classification," *Applied Intelligence*, vol. 50, no. 8, pp. 2488–2502, Aug. 2020, doi: 10.1007/s10489-020-01637-z.
- [28] A. Ramaswamy and E. Hüllermeier, "Deep q-learning: Theoretical insights from an asymptotic analysis," *IEEE Transactions on Artificial Intelligence*, vol. 3, no. 2, pp. 139–151, Sept. 2022.
- [29] Y. Zhang, Z. Zhang, Q. Yang, D. An, D. Li, and C. Li, "EV charging bidding by multi-DQN reinforcement learning in electricity auction market," *Neurocomputing*, vol. 397, pp. 404–414, Jul. 2020, doi: 10.1016/j.neucom.2019.08.106.



Sveinung Attestog received B.Sc. and M.Sc. degrees in Renewable Energy and Ph.D. in Engineering with specialisation in Mechatronics from University of Agder, Grimstad, Norway in 2016, 2018 and 2022, respectively. His main research interests include modelling and fault diagnosis of PMSM in dynamic operating conditions.



Jagath Sri Lal Senanayaka (M'20) received the B.Sc. degree in electrical and information engineering from the University of Ruhuna, Galle, Sri Lanka, in 2007, the M.B.A. degree in technology management from the University of Moratuwa, Moratuwa, Sri Lanka, in 2012, and the M.Sc. degree in renewable energy and Ph.D. degree in mechatronics from the University of Agder, Grimstad, Norway, in 2014 and 2020, respectively. From 2021 to 2022, he was a Post doctoral Research Fellow with the University of Agder.

Currently, he is an Associate Professor with the Faculty of Science and Technology at Norwegian university of life sciences(NMBU). His current research interests include fault diagnosis and control of electric powertrains, power electronics and renewable energy.



Huynh Van Khang received the B.Sc. degree in electrical engineering from the Ho Chi Minh City University of Technology, Ho Chi Minh City, Vietnam, in 2002, the M.Sc. degree in electrical engineering from Pusan National University, Busan, South Korea, in 2008, and the D.Sc. (Tech.) degree in electrical engineering from Aalto University, Espoo, Finland, in 2012. He was an Associate Professor in electrical power engineering with the University of Agder, Grimstad, Norway, from 2013 to 2019, where he is currently a

Professor with the Department of Engineering Sciences. His research interests include electrical machines, condition-based maintenance, and applied power electronics.



Kjell G. Robbersmyr (M'15–SM'16) received the M.Sc. and Ph.D. degrees in mechanical engineering from the Norwegian University of Science and Technology, Trondheim, Norway, in 1985 and 1992, respectively. He is a Professor of Machine design. Earlier, he was the head of Dynamics Research Group, and he is currently a Director of Top Research Centre Mechatronics with the University of Agder, Grimstad, Norway. His main research interests include machine design, rotating machines, condition monitoring

and vehicle crash simulations.